CMS Physics Analysis Summary

Contact: cms-pag-conveners-susy@cern.ch 2018/03/19

Search for chargino pair production and top squark pair production in final states with two leptons in proton-proton collisions at $\sqrt{s} = 13$ TeV

The CMS Collaboration

Abstract

A search for pair production of supersymmetric particles in events with two leptons (electrons or muons) and missing transverse momentum is reported. The data sample corresponds to 35.9 fb^{-1} of proton-proton collisions at $\sqrt{s} = 13$ TeV collected by the CMS detector during the 2016 data taking period at the CERN LHC. The search targets two signal models for chargino and top squark pair production. No significant deviation is observed from the predicted background. The results are interpreted in terms of several simplified models assuming R-parity conservation and with the neutralino as the lightest supersymmetric particle. When the chargino is assumed to undergo a cascade decay through sleptons, exclusion limits at 95% confidence level are set on the mass of the chargino up to 800 GeV and on the mass of the neutralino up to 320 GeV. For the top squark production, the search focuses on models with a small mass difference between the top squark and the lightest neutralino. When the top squark decays into an off-shell top quark and a neutralino, the limits extend up to 420 and 360 GeV for the top squark and neutralino masses, respectively.

1 Introduction

The standard model (SM) has been able to describe particle physics phenomena with outstanding precision up to date. However, the SM faces several issues, including the hierarchy problem between the Higgs boson mass and the Planck scale, and the lack of a dark matter candidate to explain cosmological observations [1–3]. Supersymmetry (SUSY) [4–11] is an extension of the SM that assigns a fermion (boson) superpartner to every SM boson (fermion). This theory can solve the hierarchy problem since the large quantum loop corrections to the Higgs boson mass, due mainly to the top quark, can be compensated by the analogous corrections from the top quark superpartner [12–15]. Moreover, if R-parity [16] is conserved, the lightest supersymmetric particle (LSP) is stable and possibly massive, providing a good candidate for dark matter.

This note presents a search for supersymmetric particle production in final states with two oppositely charged (OC) leptons (ℓ) and missing transverse momentum stemming from LSPs. Only electrons (e) and muons (μ) are considered. The search targets two specific signal models with chargino ($\widetilde{\chi}_1^{\pm}$) and top squark ($\widetilde{\mathrm{t}}$) pair production, using 35.9 fb^{-1} of data from proton-proton (pp) collisions at a center-of-mass-energy of $\sqrt{s} = 13$ TeV collected by the CMS experiment [17] at the CERN LHC.

The results are interpreted in terms of various simplified supersymmetric model spectra (SMS) [18–20]. The search for chargino pair production considers, as reference, a model (Fig. 1, left) where the charginos decay into a lepton, a neutrino (ν), and the lightest neutralino ($\widetilde{\chi}_1^0$) via an intermediate slepton ($\widetilde{\chi}_1^{\pm} \to \nu\tilde{\ell} \to \nu\ell\widetilde{\chi}_1^0$) or sneutrino ($\widetilde{\chi}_1^{\pm} \to \ell\tilde{\nu} \to \ell\nu\widetilde{\chi}_1^0$). The three generations of sleptons are assumed to be degenerate, with a mass equal to the average of the chargino and neutralino masses. The branching fractions of the chargino decays into charged sleptons or sneutrinos are assumed to be equal. Results are also interpreted in terms of a second model (Fig. 1, right), where both charginos decay into the lightest neutralino and a W boson. Searches for chargino pair production have been previously published by the CMS Collaboration in the context of the former scenario using 8 TeV collision data [21] and by the ATLAS Collaboration in the context of both scenarios using 8 [22–24] and 13 TeV collision data [25, 26].

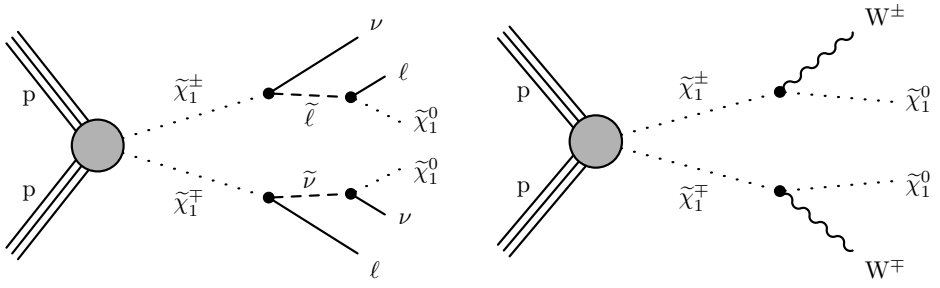

Figure 1: Diagrams of the chargino pair production in two possible decay modes: the left plot shows decays through intermediate sleptons or sneutrinos, while the right one displays decays into a W boson and the lightest neutralino.

The search for top squark pair production focuses on a SMS in which the top squark decays into a top quark and the lightest neutralino as shown in Fig. 2 (left). The analysis strategy is optimized for a compressed scenario where the mass difference between the top squark and the lightest neutralino, Δm, lays between the top quark and W boson masses $m_{\mathrm{W}} < \Delta m \lesssim m_{\mathrm{t}}$. In this regime, the top quarks are produced off-shell, giving rise to final states with relatively soft bottom quarks and W bosons. Further interpretations of the results are given in terms of

an additional model, where each of the pair produced top squarks decays into a bottom quark and a chargino, which in turn decays into a W boson and the lightest neutralino, as shown in Fig. 2 (right). In this model, the mass of the chargino is assumed to be equal to the average of the top squark and neutralino masses. This work is complementary to another OC-lepton search published by the CMS Collaboration [27], aimed at testing models where $\Delta m > m_{\mathrm{t}}$, which result in final states with on-shell top quarks and higher momentum particles. The CMS Collaboration has also published other searches targeting the same signal models in final states with exactly one lepton [28] and no leptons [29], with the latter also covering the four-body-decay of the top squark in the region $\Delta m < 80\,\mathrm{GeV}$. The ATLAS Collaboration published several searches addressing these signal models using all three final states [30–32].

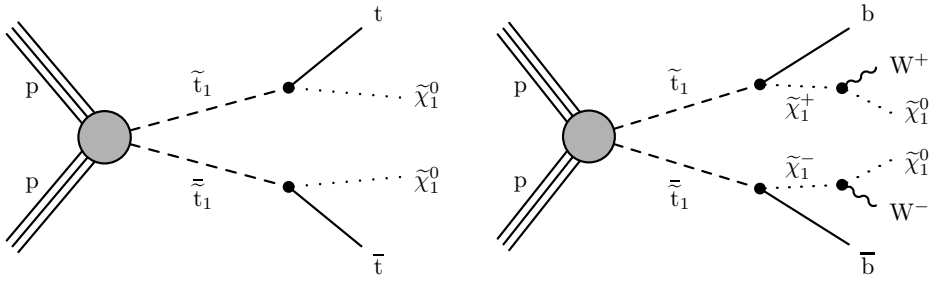

Figure 2: Diagrams of the top squark-antisquark pair production with two possible decay modes for the top squark: the left plot shows decays into a top quark and the lightest neutralino, while the right one displays decays into a bottom quark and a chargino further decaying into a neutralino and a W boson.

The note is organized as follows: Section 2 introduces the experimental apparatus; Sections 3 and 4 describe the data and simulated event samples used in this search and the details on the reconstruction of the physics objects, respectively; Section 5 exposes the general strategy of the analysis; Sections 6 and 7 discuss the estimates of the contributions from SM processes to the selected events and the sources of their systematic uncertainties, respectively; Section 8 shows the results and their interpretation in terms of the considered SMS; and finally Section 9 summarizes the results of the search.

2 The CMS detector

The central feature of the CMS apparatus is a superconducting solenoid of 6 m internal diameter, providing a magnetic field of 3.8 T. Within the solenoid volume are a silicon pixel and strip tracker, a lead tungstate crystal electromagnetic calorimeter (ECAL), and a brass and scintillator hadron calorimeter (HCAL), each composed of a barrel and two endcap sections. Forward calorimeters extend the pseudorapidity (η) coverage provided by the barrel and endcap detectors. The tracker and calorimeter systems allow the reconstruction of electrons and hadronic jets. Muons are detected in gas-ionization chambers embedded in the steel flux-return yoke outside the solenoid. The detector is nearly hermetic, allowing for momentum balance measurements in the plane transverse to the beam direction. A more detailed description of the CMS detector, together with a definition of the coordinate system used and the relevant kinematic variables, can be found in Ref. [17].

3 Data samples

Events of interest are selected during data taking using a two-tiered trigger system [33]. The events are triggered by requiring the presence of two leptons (ee, $\mu\mu$, eμ). The threshold on the transverse momentum (p_T) of the leading lepton is 23 GeV for ee and eμ triggers, and 17 GeV for $\mu\mu$ triggers. The threshold for the trailing lepton is 8 TeV for muons and 12 GeV for electrons. To increase the efficiency of the trigger selection, events are also accepted by triggers requiring at least one lepton with higher p_T and tighter identification criteria. The efficiency of the trigger selection is measured in a sample of reconstructed $Z \to \ell^+\ell^-$ decays and is found to range between 90 and 99% depending on the transverse momentum and pseudorapidity of the leptons.

Samples of Monte Carlo (MC) simulated events are used to study the contribution of SM processes to the selected data set and the expected acceptance for the different signal models. Events from top quark pair production ($t\bar{t}$) are generated with POWHEG v2 [34–36] and normalized to the expected cross section calculated at next-to-next-to-leading order (NNLO) in perturbative quantum chromodynamics (QCD) [37]. Events with a single top quark produced in association with a W boson (tW) are generated with POWHEG v1 [38] and normalized to the NNLO cross section. Diboson production (WW, WZ, and ZZ) through quark-antiquark annihilation and gluon fusion is simulated using POWHEG v2 [39, 40] and MCFM v7 [41], respectively. The cross sections used to normalize events for the former mechanism are calculated at NNLO for WW production and at next-to-leading order (NLO) for ZZ and WZ production. Events from $q\bar{q} \to ZZ$ production are further reweighted through NNLO/NLO k-factors as a function of the generated ZZ system mass. Two additional sets of k-factors as a function of the generated ZZ system transverse momentum and of the azimuthal distance between the Z bosons are used to set an uncertainty on ZZ production. For diboson production through gluon fusion, leading-order (LO) cross sections are obtained from the MCFM generator and are corrected by NNLO/LO k-factors. Drell-Yan events are generated with MADGRAPH5_aMC@NLO [42] at LO, and normalized to the NNLO cross section [43]. Events from $t\bar{t}W$, $t\bar{t}Z$, triboson, and H$\to$WW production are generated with MADGRAPH5_aMC@NLO at NLO, and normalized to the respective NLO cross sections [44, 45]. Chargino pair production and top squark pair production events are generated using MADGRAPH5_aMC@NLO at LO with up to two extra partons, and are normalized to the respective cross sections computed at NLO plus next-to-leading logarithmic (NLL) precision [46–54] with all the other sparticles assumed to be heavy and decoupled. In the case of chargino pair production, calculations are performed in a limit of mass-degenerate wino $\widetilde{\chi}_2^0$ and $\widetilde{\chi}_1^{\pm}$, and light bino $\widetilde{\chi}_1^0$.

All processes are generated using the NNPDF3.0 [55] parton distribution function (PDF) set. The parton showering, hadronization, and the underlying event are modeled using PYTHIA 8.2 [56] with the CUETP8M1 [57] underlying event tune for all of processes, except in the generation of $t\bar{t}$ events, where the first emission is done at the matrix element level with POWHEG v2 and the CUETP8M2T4 tune is used. Weights for the estimation of theoretical systematic uncertainties, including those related to the choice of the PDF sets and QCD scale, are included in simulated events [58].

The detector response on the generated events is simulated using a realistic model of the CMS detector based on GEANT4 [59] for SM processes, while for signal events a fast simulation (FastSim) [60] of the detector based on a parametrization of the average response to particles is used. Simulated events are subsequently reconstructed using the same reconstruction algorithms applied on data.

In order to model the effect of multiple interactions per bunch crossing (pileup), simulated

events are mixed with simulated minimum bias events, and are reweighted in order to match the rate of multiple interactions observed in data.

To improve the modeling of initial-state radiation (ISR) in simulated signal events, reweighting factors are applied as to make the distribution of suitable observables agree with data. For chargino pair production, mediated by electroweak interaction, the reweighting procedure is based on studies of transverse momentum balance in inclusive Z boson production events [61]. Events are then reweighted according to the total transverse momentum ($p_{\mathrm{T}}^{\mathrm{ISR}}$) of the system of SUSY particles. The reweighting factors range between 1.18 at $p_{\mathrm{T}}^{\mathrm{ISR}} \approx 125\,\mathrm{GeV}$ and 0.78 for $p_{\mathrm{T}}^{\mathrm{ISR}} > 600\,\mathrm{GeV}$. A global reweighting is further applied in order not to alter the signal production cross section. As the top squark pair production happens via strong interactions, a different set of reweighting factors is derived as a function of the multiplicity of ISR jets ($N_{\mathrm{jet}}^{\mathrm{ISR}}$) in a sample of $\mathrm{t\bar{t}}$ events selected by requiring an election-muon pair and two jets identified as coming from bottom quark hadronization. The measured reweighting factors vary between 0.92 and 0.51 for $N_{\mathrm{jet}}^{\mathrm{ISR}}$ between 1 and 6, with an additional scale factor applied to keep invariant the total number of produced events.

4 Event reconstruction

The particle-flow (PF) event algorithm [62] reconstructs and identifies each individual particle with an optimized combination of information from the various elements of the CMS detector. The energy of electrons is determined from a combination of the electron momentum at the primary interaction vertex as determined by the tracker, the energy of the corresponding ECAL cluster, and the energy sum of all bremsstrahlung photons spatially compatible with originating from the electron track. The energy of muons is obtained from the curvature of the corresponding track. The energy of charged hadrons is determined from a combination of their momentum measured in the tracker and the matching ECAL and HCAL energy deposits, corrected for zero-suppression effects and for the response function of the calorimeters to hadronic showers. Finally, the energy of neutral hadrons is obtained from the corresponding corrected ECAL and HCAL energy.

The reconstructed vertex with the largest value of summed physics-object p_{T}^2 is taken to be the primary pp interaction vertex. The physics objects are the jets, clustered using a jet finding algorithm [63, 64] with the tracks assigned to the vertex as inputs, and the associated missing transverse momentum, taken as the negative vector sum of the p_{T} of those jets.

The identification of the muons used in the analysis is based on the number of reconstructed deposits in the tracker and in the muon system, and on the fit quality of the muon track. Electron identification relies on quality criteria on the electron track, matching between the electron trajectory and the associated cluster in the calorimeter, and shape observables of the electromagnetic shower observed in the ECAL.

The lepton selection is further optimized to select leptons from the decay of W or Z bosons. The leptons are required to be isolated by measuring their relative isolation (I_{rel}), as the ratio of the scalar p_{T} sum of the photons and of the neutral and charged hadrons within a cone of radius $R = \sqrt{(\Delta\phi)^2 + (\Delta\eta)^2} = 0.3$ around the candidate lepton, and the p_{T} of the lepton itself. The contribution of particles produced in pileup interactions is reduced by considering only charged hadrons consistent with originating from the primary vertex of the event, and correcting for the expected contribution of neutral hadrons from pileup [65, 66]. Leptons are considered to be isolated if their relative isolation I_{rel} is found to be smaller than 0.12. A looser requirement of $I_{\mathrm{rel}} < 0.4$ is also used to define a veto lepton selection. Candidate lep-

ton trajectories are further required to be compatible with the primary interaction vertex by imposing constraints on their transverse (d_0) and longitudinal (d_z) impact parameters, and on the three-dimensional impact parameter significance (S_d^{3D}), computed as the ratio of the three-dimensional impact parameter and its uncertainty. Both electrons and muons are required to satisfy the conditions $|d_0| < 0.05$ cm, $|d_z| < 0.1$ cm, and $S_d^{3D} < 4$. Finally, electrons originating from photon conversions are rejected by requiring the electron track not to have missing hits in the innermost layers of the tracker, and not to form a good conversion vertex with any other candidate electron in the event [65].

For each event, hadronic jets are clustered from the PF reconstructed particles using the infrared and collinear safe anti-k_T algorithm [63, 64] with a distance parameter of 0.4. The jet momentum is determined as the vectorial sum of all particle momenta in the jet, and is found in the simulation to be within 5 to 10% of the true momentum over the whole p_T spectrum and detector acceptance. Jet energy corrections are derived from the simulation, and are confirmed with in situ measurements of the energy balance in dijet and photon + jet events [67]. Loose requirement on jet energy fraction and multiplicity variables are applied to reject spurious jets from detector noise. Finally, the jets overlapping with any selected lepton within a cone of radius $R < 0.4$ are removed.

Jets originating from the hadronization of bottom quarks (b jets) are identified by the combined secondary vertex v2 (CSVv2) b tagging algorithm, using the medium operating point [68]. This requirement provides an efficiency for identifying b jets increasing from 50% to 70% for jets with transverse momentum from 20 to 100 GeV, with a misidentification rate for jets originating from light quarks and gluons of about 1% in the same p_T range.

The energy imbalance of the event in the transverse plane is denoted as missing transverse momentum ($\vec{p}_T^{\,miss}$) and it is estimated as the negative vectorial sum of the transverse momentum of all PF candidates in the event, corrected to take into account the energy corrections applied to the jets. The magnitude of the missing transverse momentum is denoted as p_T^{miss}.

To study the effects of the modeling of the missing transverse momentum in FastSim events, the acceptance for signal events is computed both using the $\vec{p}_T^{\,miss}$ at generation level and after the global event reconstruction. The average value of the two acceptances in each analysis bin is taken as the central value for the acceptance.

Simulated events are reweighted to account for differences with respect to data in the efficiencies of the lepton reconstruction, identification, and isolation requirements, and in the performance of b jet identification. The values of these data-to-simulation scale factors differ from unity by less than 10% with typical efficiency corrections of 2-3% (5%) for the identification of leptons (b jets) with $p_T > 20$ GeV.

5 Search strategy

The search strategy is developed for two kind of signals: the chargino pair production, studied along the whole ($m_{\tilde{\chi}_1^\pm}$,$m_{\tilde{\chi}_1^0}$) mass plane, and the top squark pair production, focused on the compressed scenario where the mass difference of the top squark and the lightest neutralino is in between the top quark and W boson masses. The searches involve the same techniques for the background estimation and the signal extraction while they differ slightly in the signal region selection in order to improve their respective sensitivity.

The considered signal models are characterized by a common final state with two OC leptons and two lightest neutralinos contributing to large missing transverse momentum. Based on

this, a general high-acceptance baseline selection is defined, requiring two isolated leptons with opposite charge, pseudorapidity $|\eta| < 2.4$, and transverse momentum $p_T \geq 25$ (20) GeV for the leading (trailing) lepton. To reduce the contributions from low-mass resonance and Drell-Yan production, the invariant mass $m_{\ell\ell}$ of the lepton pair is required to be greater than 20 GeV, and if both leptons have the same flavor (SF), $m_{\ell\ell}$ is further required to satisfy $|m_{\ell\ell} - m_Z| > 15$ GeV, where m_Z is the Z boson mass. High missing transverse momentum $p_T^{miss} > 140$ GeV is required. Events are further rejected if they contain a third lepton with $p_T > 15$ GeV, $|\eta| < 2.4$, and satisfying the veto lepton selection (Section 4). A summary of the baseline selection is found in Table 1.

Table 1: Definition of the baseline selection used in the searches for chargino pair production and top squark pair production.

Variable	Selection
lepton flavor	e^+e^-, $\mu^+\mu^-$, $e^\pm\mu^\mp$
third lepton veto	$p_T > 15$ GeV, $\|\eta\| < 2.4$
leading lepton p_T	≥ 25 GeV, $\|\eta\| < 2.4$
trailing lepton p_T	≥ 20 GeV, $\|\eta\| < 2.4$
$m_{\ell\ell}$	≥ 20 GeV
$\|m_{\ell\ell} - m_Z\|$	> 15 GeV only for ee and $\mu\mu$ events
p_T^{miss}	≥ 140 GeV

The SM processes that contribute most after the baseline selection are $t\bar{t}$, tW, and WW productions. For all these backgrounds, the lepton pair and the missing transverse momentum come from a W boson pair. Consequently, if we construct the stransverse mass variable M_{T2} [69], which generalizes the transverse mass (M_T) for a system with two invisible particles, by using the two leptons as the two visible systems:

$$M_{T2}(\ell\ell) = \min_{\vec{p}_T^{miss1} + \vec{p}_T^{miss2} = \vec{p}_T^{miss}} \left(\max \left[M_T(\vec{p}_T^{lep1}, \vec{p}_T^{miss1}), M_T(\vec{p}_T^{lep2}, \vec{p}_T^{miss2}) \right] \right), \quad (1)$$

we obtain an observable whose distribution for the considered backgrounds reaches a kinematic endpoint at the W boson mass. Signal events, instead, present stransverse mass spectra without such an endpoint because of the additional contribution given by the neutralinos to $\vec{p}_T^{miss}$. The sensitivity of the analysis is further enhanced by dividing the signal region in bins of missing transverse momentum. This allows not only to exploit the larger tails in the p_T^{miss} distribution of the signal events, but also to optimise the sensitivity to signals with different mass separation between the produced supersymmetric particle and the LSP. Each p_T^{miss} bin is in turn divided into events with SF and different flavor (DF) leptons to exploit the smaller contamination from WZ, ZZ, and Drell-Yan production of the latter.

The signal regions are further subdivided based on the specific characteristics of each signal model. A veto on b-tagged jets is applied to reject $t\bar{t}$, tW, and $t\bar{t}Z$ events in the chargino search. While not providing sensitivity for the signal production, events with b-tagged jets are kept as a control region for the normalization of the background from $t\bar{t}$ and tW production (see Section 6). Events without b-tagged jets are in turn split in two sub-regions with or without a jet ($p_T > 20$ GeV, $|\eta| < 2.4$) in the p_T^{miss} bins below 300 GeV, to exploit the larger fraction of signal events with no jets with respect to top background that still contaminate the signal region after applying the b-tag veto requirement.

The final states produced in the top squark decays are characterized by the presence of two bottom quarks. When the difference in the mass of the top squark and the neutralino is small,

the bottom quarks are soft and give rise to jets with relatively low momentum that have a lower probability to be tagged. In this case, the top squark final states are similar as in the chargino pair production and requiring a veto on b-tagged jets is again an effective strategy to define signal regions with reduced contamination from $t\bar{t}$, tW, and $t\bar{t}Z$ backgrounds. As the mass difference between the top squark and the neutralino becomes larger, however, the fraction of signal events with b-tagged jets increases and the signal becomes more $t\bar{t}$-like. In these conditions, a b-tag requirement improves the sensitivity to top squark production by reducing the background from diboson and Drell-Yan events.

Another useful handle to discriminate top squark production from SM processes is given by the presence in the events of high-p_T jets from ISR. The invisible particles (neutrinos and neutralinos) produced in the decay chain of the top squark in the compressed scenario are expected to be soft; events with more hard neutralinos, however, can arise when the top squark pair system recoils against a high-p_T ISR jet. In this high ISR regime, background is still constrained by the kinematic W mass endpoint in $M_{T2}(\ell\ell)$, and can be effectively separated from signal. High ISR events are selected by requiring the leading jet to have $p_T > 150\,\text{GeV}$ and not to be b-tagged. In order to favor the topology in which the jet recoils against the rest of the system, the separation in azimuthal angle between the jet and the $\vec{p}_T^{\,\text{miss}}$ is required to be larger than 2.5 rad. This requirement is found to be effective in discriminating top squark production from background events at high p_T^{miss}, and is therefore applied only for events with $p_T^{\text{miss}} > 300\,\text{GeV}$.

A summary of the signal regions for the chargino and top squark searches is given in Tables 2 and 3, respectively, indicating the p_T^{miss} range, the selection on the multiplicity of jets (n_{jets}) and b jets ($n_{\text{b jets}}$) in the event, and the ISR jet requirement.

Table 2: Definition of the signal regions for the chargino search as a function of the b jet multiplicity, ISR jet requirement, and the p_T^{miss} value. Also shown are the control regions with b-tagged jets used for the normalization of the $t\bar{t}$ and tW backgrounds. Each of the regions is further divided in seven $M_{T2}(\ell\ell)$ bins.

	$SR1^{0Jet}_{0Tag}$	$SR1^{Jets}_{0Tag}$	$CR1_{Tags}$	$SR2^{0Jet}_{0Tag}$	$SR2^{Jets}_{0Tag}$	$CR2_{Tags}$	$SR3_{0Tag}$	$CR3_{Tags}$
Channel	SF, DF	SF, DF	SF, DF	SF, DF	SF, DF	SF, DF	SF, DF	SF, DF
n_{jets}	0	≥ 1	≥ 1	0	≥ 1	≥ 1	≥ 0	≥ 1
$n_{\text{b jets}}$	0	0	≥ 1	0	0	≥ 1	0	≥ 1
p_T^{miss} [GeV]	140-200	140-200	140-200	200-300	200-300	200-300	$\geq$300	$\geq$300
ISR jets	≥ 0	≥ 0	≥ 0	≥ 0	≥ 0	≥ 0	≥ 0	≥ 0
$M_{T2}(\ell\ell)$	0-20, 20-40, 40-60, 60-80, 80-100, 100-120, $\geq 120\,\text{GeV}$							

Each of the signal regions defined in Tables 3 and 2 is further divided in seven $M_{T2}(\ell\ell)$ bins of 20 GeV, starting from 0 GeV and with the last bin collecting all events with $M_{T2}(\ell\ell) > 120\,\text{GeV}$. A simultaneous maximum likelihood (ML) fit to the $M_{T2}(\ell\ell)$ distributions is then performed to extract the signal (see Section 8). Since the first $M_{T2}(\ell\ell)$ bins have a low signal contribution, we exploit them to constrain the contributions of the dominant backgrounds in the signal regions with one b-tagged jet (dominated by $t\bar{t}$ and tW production) and without b-tagged jets (where WW production becomes relevant) through the fit itself.

Table 3: Definition of the signal regions for the top squark production search as a function of the b jet multiplicity, ISR jet requirement, and $p_{\mathrm{T}}^{\mathrm{miss}}$ value. Each of the regions is further divided in seven $M_{\mathrm{T2}}(\ell\ell)$ bins.

	$\mathrm{SR1}_{\mathrm{0Tag}}$	$\mathrm{SR1}_{\mathrm{Tags}}$	$\mathrm{SR2}_{\mathrm{0Tag}}$	$\mathrm{SR2}_{\mathrm{Tags}}$	$\mathrm{SR3}^{\mathrm{ISR}}_{\mathrm{0Tag}}$	$\mathrm{SR3}^{\mathrm{ISR}}_{\mathrm{Tag}}$
Channel	SF, DF	SF, DF	SF, DF	SF, DF	SF, DF	SF, DF
n_{jets}	≥ 0	≥ 1	≥ 0	≥ 1	≥ 1	≥ 2
$n_{\mathrm{b\,jets}}$	0	≥ 1	0	≥ 1	0	≥ 1
$p_{\mathrm{T}}^{\mathrm{miss}}$ [GeV]	140-200	140-200	200-300	200-300	≥ 300	≥ 300
ISR jets	≥ 0	≥ 0	≥ 0	≥ 0	≥ 1	≥ 1
$M_{\mathrm{T2}}(\ell\ell)$	0-20, 20-40, 40-60, 60-80, 80-100, 100-120, ≥ 120 GeV					

6 Background estimation

The main contributions from SM processes to the signal regions comes from $\mathrm{t\bar{t}}$, tW, and WW production. The normalization of these backgrounds is determined by the ML fit, as mentioned in Section 5. Their $M_{\mathrm{T2}}(\ell\ell)$ shape has a natural endpoint at the W boson mass, and the events that enter in the relevant region for signal extraction ($M_{\mathrm{T2}}(\ell\ell)$ >80 GeV) are mainly due to detector resolution effects, whose contribution is not easy to model. For this reason, we study the modeling of the $M_{\mathrm{T2}}(\ell\ell)$ distribution for these processes in dedicated data control regions (see Section 6.1). The contribution of the subleading $\mathrm{t\bar{t}Z}$, WZ, ZZ, and Drell-Yan backgrounds is also tested in control regions where correction factors for their normalization are extracted (see Section 6.2). The rest of the SM processes are found to give minor contributions in the signal regions, and the estimates for these processes are taken directly from simulation. The contribution of signal to any of the control regions used is found to be negligible compared to SM processes.

6.1 Modeling of $M_{\mathrm{T2}}(\ell\ell)$ in $\mathrm{t\bar{t}}$, tW, and WW events

The simulated $M_{\mathrm{T2}}(\ell\ell)$ distributions for $\mathrm{t\bar{t}}$, tW, and WW backgrounds are validated in two control regions. To construct the first one, the baseline selection is modified by requiring $100 < p_{\mathrm{T}}^{\mathrm{miss}} < 140$ GeV. The selected events are further separated according to their b jet multiplicity to define two regions with different content in top ($\mathrm{t\bar{t}}$ and tW) and WW backgrounds. In order to reject events from Drell-Yan production, only DF events are considered. The second control region aims at validating the modeling of the $M_{\mathrm{T2}}(\ell\ell)$ distributions in events with $p_{\mathrm{T}}^{\mathrm{miss}} > 140$ GeV. At this purpose, we select events from $\mathrm{WZ} \to 3\ell 1\nu$ production and emulate the $M_{\mathrm{T2}}(\ell\ell)$ shape of WW and top events. We take the lepton from the Z boson with the same charge as the lepton from the W boson, and we add its transverse momentum vectorially to $\vec{p}_{\mathrm{T}}^{\mathrm{miss}}$, effectively treating it like a neutrino. These events are selected by requiring three leptons and vetoing the presence of a fourth lepton passing the lepton veto requirements. A veto is applied on events with b-tagged jets to remove residual $\mathrm{t\bar{t}}$ events. Among the three leptons, a pair of OCSF leptons with an invariant mass within 10 GeV from the Z boson mass is required to identify the Z boson. The simulation is found to describe the data well in the control regions. Based on the statistical precision of these control regions, a conservative uncertainty of 5, 10, 20, and 30% is taken for the bins $60 \leq M_{\mathrm{T2}}(\ell\ell) < 80$ GeV, $80 \leq M_{\mathrm{T2}}(\ell\ell) < 100$ GeV, $100 \leq M_{\mathrm{T2}}(\ell\ell) < 120$ GeV, and $M_{\mathrm{T2}}(\ell\ell) > 120$ GeV, respectively. These uncertainties are applied to top and WW production, and treated as uncorrelated between the two types of backgrounds.

Another potential source of mis-modeling in the tails of the $M_{\mathrm{T2}}(\ell\ell)$ distributions arises from nonprompt leptons, originating for instance from semileptonic decays of B hadrons in b jets or from hadronic jets accidentally passing the lepton selection. The value of $M_{\mathrm{T2}}(\ell\ell)$ in $\mathrm{t\bar{t}}$, tW, and WW events with one nonprompt lepton replacing a prompt one failing the selection requirements will not be bound by the W mass endpoint. The contribution of these events is found to be lower than 1% of the expected background across the different signal regions. They become more relevant only at large values of $M_{\mathrm{T2}}(\ell\ell)$ and $p_{\mathrm{T}}^{\mathrm{miss}}$, where they constitute up to 20% of the $\mathrm{t\bar{t}}$ background. We study the modeling of the rate of nonprompt leptons in simulation by selecting events with two leptons with the same charge and at least one b-tagged jet. The dominant contribution to this sample comes from $\mathrm{t\bar{t}}$ events with a nonprompt lepton. Based on the observed agreement with data, a correction factor of 1.08 ± 0.21 is derived for the nonprompt lepton rate in simulation.

6.2 Normalization of $t\bar{t}Z$, WZ, ZZ, and Drell-Yan backgrounds

The production of $t\bar{t}Z$ events where the two W bosons decay leptonically and the Z boson decays into neutrinos leads to final states with the same experimental signature as the signal events and with no natural endpoint for the reconstructed $M_{T2}(\ell\ell)$ distribution, due to the additional contribution of the neutrinos from the Z boson decay to the $\vec{p}_T^{\,miss}$. The normalization of this background is validated in events with three leptons, $p_T^{miss} > 140\,GeV$, and at least two jets with $p_T > 20\,GeV$ of which at least one is tagged as a b jet. At least one pair of OCSF leptons with an invariant mass not further than 10 GeV from the Z boson mass is also required. A normalization scale factor of 1.44 ± 0.36 for $t\bar{t}Z$ production is measured comparing the observed and predicted number of events.

Events from WZ production enter the signal event selection when both bosons decay leptonically and one of the three produced leptons fails the veto lepton requirements. We test the modeling of this source of background in a control region with three leptons, $p_T^{miss} > 140\,GeV$ and no b-tagged jets, and derive a normalization scale factor of 0.97 ± 0.09.

The ZZ background is dominated by events with one boson decaying into charged leptons and the other one decaying into neutrinos. This contribution is studied by mimicking the $ZZ \to 2\ell 2\nu$ production through $ZZ \to 4\ell$ events, where the transverse momentum of one of the reconstructed Z bosons (randomly chosen between the ones satisfying the $|m_{\ell\ell} - m_Z| < 15\,GeV$ condition) is added to the $\vec{p}_T^{\,miss}$. Events are selected by requiring four leptons, with one lepton allowed to pass the looser veto lepton requirement in order to increase the acceptance for ZZ production. The events are retained if the four leptons can be arranged into two pairs of OCSF leptons, both with an invariant mass within 30 GeV from the Z boson mass, and at least one within 15 GeV. A scale factor for the ZZ background normalization is derived in events with $p_T^{miss} > 140\,GeV$ and with no b-tagged jets. Since the chargino search uses separate signal regions for events with or without jets, two corresponding scale factors are also measured. A summary of the scale factors derived in this section is given in Table 4. For all the quoted scale factor, uncertainties include the statistical uncertainties on data and simulated events, and the systematic uncertainties on the purity of the control regions.

Drell-Yan events can pass the baseline selection because of mismeasurements in the missing transverse momentum. We study the modeling of this background in events with two OCSF leptons with $|m_{\ell\ell} - m_Z| < 15\,GeV$, no additional leptons, and no b-tagged jets (Z-peak events). The events with $100 < p_T^{miss} < 140\,GeV$ are dominated by Drell-Yan production, and are used to derive a $M_{T2}(\ell\ell)$ shape correction, which is subsequently tested in Z-peak events with $p_T^{miss} > 140\,GeV$. The correction ranges from a few percent at low $M_{T2}(\ell\ell)$ to about 50% for $M_{T2}(\ell\ell) > 100$ GeV. An overall normalization uncertainty of 32% is also established by the observed disagreement in data and simulated events with $100 < p_T^{miss} < 140\,GeV$. Finally, the predictions for Drell-Yan events with no jets are tested in Z-peak events with no jets and $p_T^{miss} > 140\,GeV$: a conservative uncertainty of 100% on this contribution is applied. The Drell-Yan production is a subdominant background in the signal regions with no jets and this uncertainty has a negligible impact on the expected sensitivity for signal production.

7 Systematic uncertainties

Several sources of systematic uncertainty that affect both the normalization and the $M_{T2}(\ell\ell)$ shape of the background and signal events are considered in the analysis.

- A background normalization uncertainty is applied on each background separately.

Table 4: Summary of the normalization scale factors for $t\bar{t}Z$, WZ, and ZZ backgrounds in the signal regions used for the chargino (a) and top squark (b) searches. Uncertainties include the statistical uncertainties on data and simulated events, and the systematic uncertainties on the purity on the control regions.

Process	Scale factors		
	$N_{jets} = 0$ (a)	$N_{jets} > 0$ (a)	$N_{jets} \geq 0$ (b)
$t\bar{t}Z$	1.44 ± 0.36	1.44 ± 0.36	1.44 ± 0.36
WZ	0.97 ± 0.09	0.97 ± 0.09	0.97 ± 0.09
ZZ	0.74 ± 0.19	1.21 ± 0.17	1.05 ± 0.12

The normalization of the $t\bar{t}$, tW, and WW processes is determined by the ML fit, as described in Section 8. We assign a common normalization parameter for $t\bar{t}$ and tW events and another for WW production. No explicit normalization uncertainty is defined for $t\bar{t}$ and WW events, while a 10% uncertainty is set for the tW process to take into account the relative normalization with respect to $t\bar{t}$ production. The uncertainties applied to $t\bar{t}Z$ (25%), WZ (8%), and ZZ (26% in the signal regions with 0 jets, 14% in the signal regions with at least 1 jet, and 11% in the rest of signal regions) correspond to the scale factors obtained in Section 6. Minor backgrounds ($t\bar{t}W$, H$\rightarrow$WW, VVV) are given a conservative uncertainty of 50%. Finally, Drell-Yan events have a 100% normalization uncertainty in the signal region with no jets and 32% in all other signal regions.

- The uncertainty on the rate of events with no jets for the diboson and jet enriched ($t\bar{t}$, tW, ttV) backgrounds is introduced in the fit through two free parameters normalizing the yields of events with no jets for these two classes of processes, respectively. The total number of events expected for each process in the two signal regions with and without jets is constrained to remain invariant, so that only a migration of events from these two regions is allowed.
- The overall uncertainty in the integrated luminosity delivered to the CMS experiment during the 2016 LHC run is estimated to be 2.5% [70].
- Lepton identification and isolation efficiencies are corrected by data-to-simulation scale factors measured in Z$\rightarrow \ell\ell$ events. The corresponding uncertainties are typically smaller than 3% per lepton.
- The efficiencies and misidentification rates of the b jet identification algorithms are also corrected by data-to-simulation scale factors measured in inclusive jets and $t\bar{t}$ events [68]. The respective uncertainties range between 1 and 6% depending on the transverse momentum and pseudorapidity of the jet.
- The modeling of the $M_{T2}(\ell\ell)$ shapes in events with an endpoint at the W mass ($t\bar{t}$, tW and WW) has been studied in Section 6: an uncertainty of 5, 10, 20, and 30% is set for the last four $M_{T2}(\ell\ell)$ bins.
- The choice of the set of NNLO/NLO k-factors applied to the $q\bar{q} \rightarrow$ ZZ events affects the modeling of the $M_{T2}(\ell\ell)$ shape for the ZZ background (see Section 3). Relative variations range from 16% for $M_{T2}(\ell\ell) < 20$ GeV to about 2% for $M_{T2}(\ell\ell) > 120$ GeV and are taken as uncertainties.
- The $M_{T2}(\ell\ell)$ distribution in Drell-Yan events has been corrected by $M_{T2}(\ell\ell)$-dependent scale factors derived in the validation region $100 < M_{T2}(\ell\ell) < 140$ GeV to account for the observed mismodeling of Drell-Yan simulated events. The full size of the

correction in each bin is taken as an uncertainty.

- The weight of events with nonprompt leptons in simulated samples is varied by the $\pm$19% uncertainty in the correction factor derived in events with two leptons of same charge, as described in Section 6.1.
- A flat uncertainty of 2% on the trigger efficiencies is applied.
- The jet energy scale is varied by its uncertainty, and the changes are propagated to all the related observables in the event.
- The unclustered energy is varied by its uncertainty, and the changes are propagated to the missing transverse momentum.
- The spectrum of top quark p_{T} in $\mathrm{t\bar{t}}$ events has been observed to be softer in data than in simulated events [71–73]. An uncertainty is derived by the observed variations when reweighting the $\mathrm{t\bar{t}}$ events to the p_{T} distribution observed in data.
- Simulated signal events are reweighted to improve the modeling of the initial-state radiation, as described in Section 3. For chargino models, the deviation from unity is taken as the systematic uncertainty in the $p_{\mathrm{T}}^{\mathrm{ISR}}$ reweighting factors. For top squark models, half of the deviation from unity in the $N_{\mathrm{jet}}^{\mathrm{ISR}}$ factors is taken.
- The effect of the simulated sample statistics on the modeling of the $M_{\mathrm{T2}}(\ell\ell)$ distributions is taken into account by treating the statistical uncertainty in each bin for each process as an additional uncorrelated uncertainty.
- The modeling of the missing transverse momentum in FastSim events is studied by comparing the acceptances computed using the $\vec{p}_{\mathrm{T}}^{\,\mathrm{miss}}$ at generation level and after the global event reconstruction. One-half the difference between the two values is taken as an uncertainty, fully correlated among bins.
- An uncertainty in the modeling of pileup events in FastSim signal samples is derived by studying the dependence of the acceptance on the multiplicity of primary vertices reconstructed in the event. This uncertainty varies from 0 to 10% across the signal regions and $M_{\mathrm{T2}}(\ell\ell)$ bins.
- Uncertainties in QCD scale and PDFs are propagated by taking the largest changes in the acceptance when doubling and halving the renormalization and factorization scales, and when varying the choice of PDFs between the NNPDF3.0 member sets. The PDF uncertainties are not considered for signal models as they are found to be redundant with the uncertainty in the ISR modeling.

Table 5 summarizes the systematic uncertainties in the predicted yields for SM processes.

Table 5: Size of systematic uncertainties in the predicted yields for SM processes. The first column shows the range of the uncertainties in the global background normalization across the different signal regions, while the second one gives the effect on the $M_{\mathrm{T2}}(\ell\ell)$ shape.

Systematic	Change in yields	Change in $M_{\mathrm{T2}}(\ell\ell)$ shape
Luminosity	2.5%	-
Trigger	2%	-
Lepton ID and isolation	4-5%	$< 1\%$
Track reconstruction	$< 1\%$	$< 1\%$
b-tagging	0-3%	0-2%
b-tagging (light jets)	$< 1\%$	0-1%
JES	1-6%	3-15%
Unclustered energy	1-2%	2-16%
$\mathrm{t\bar{t}}$ p_{T} reweighting	1-4%	1-8%
PDFs	1-5%	2-8%
QCD scale	1-10%	1-6%
$M_{\mathrm{T2}}(\ell\ell)$ shape (Top)	-	4-18%
$M_{\mathrm{T2}}(\ell\ell)$ shape (WW)	-	1-15%
Nonprompt leptons	$< 1\%$	0-4%
ttZ normalization	$< 1\%$	0-9%
WZ normalization	$< 1\%$	0-1%
ZZ normalization	0-1%	0-5%
ZZ k-factors	-	0-3%
Drell-Yan normalization	0-4%	1-11%
$M_{\mathrm{T2}}(\ell\ell)$ shape (Drell-Yan)	-	1-13%

8 Results and interpretations

No excess over SM prediction is observed in data, and upper limits at 95% confidence level (CL) are derived on the production cross sections for the different signal models considered. The asymptotic approximation of the CLs method [74–76] is used to set the limits from a simultaneous binned ML fit of the $M_{\mathrm{T2}}(\ell\ell)$ distribution in the signal regions defined in Tables 3 and 2. Uncertainties due to signal and background normalizations are included through nuisance parameters with log-normal prior distributions, while uncertainties on the shape of the $M_{\mathrm{T2}}(\ell\ell)$ distributions are included with Gaussian prior distributions. As explained in Section 6, the normalization of the main backgrounds from top and WW production is left to be determined in the fit through the constraint provided by the low $M_{\mathrm{T2}}(\ell\ell)$ region in the events with a b-tagged jet or without tagged jets, respectively. Figures 3 and 6 compare the number of observed events in the signal regions with the expected yields from SM processes after a background-only fit. As a comparison, the expected yields for a representative signal point are given. The total expected SM contributions before the fit and after a background+signal fit are also shown. Detailed information on the yields of observed and expected yields after the background-only fit are given in Tables 6 to 9 for all dilepton final states and all signal regions.

Table 6: Observed and expected yields of DF events in the signal regions for the chargino search. The quoted uncertainty on the background predictions includes statistical and systematic contributions.

DF events	$M_{\mathrm{T2}}(\ell\ell)$ [GeV]	0-20	20-40	40-60	60-80	80-100	100-120	≥ 120
$\mathrm{SR1}^{\mathrm{Jets}}_{\mathrm{0Tag}}$	Predicted	1493 ± 32	558 ± 12	719 ± 16	730 ± 16	316 ± 10	45.1 ± 3.1	13.7 ± 2.8
	Observed	1484	532	732	725	298	47	13
$\mathrm{SR1}^{\mathrm{0Jet}}_{\mathrm{0Tag}}$	Predicted	41.9 ± 5	27.4 ± 3.8	34.1 ± 4.8	42 ± 5.5	21.1 ± 3.4	6 ± 1.3	7.9 ± 2.1
	Observed	39	24	33	44	13	6	9
$\mathrm{SR2}^{\mathrm{Jets}}_{\mathrm{0Tag}}$	Predicted	534 ± 15	158.6 ± 5.9	167.9 ± 6.1	157.9 ± 6.5	42.4 ± 2.9	5.9 ± 1	9 ± 1.7
	Observed	511	162	156	176	43	5	9
$\mathrm{SR2}^{\mathrm{0Jet}}_{\mathrm{0Tag}}$	Predicted	10.3 ± 1.7	7 ± 1.5	6.5 ± 1.3	6.9 ± 1.3	2.19 ± 0.69	1.59 ± 0.7	7.8 ± 1.8
	Observed	10	4	4	6	2	2	7
$\mathrm{SR3}_{\mathrm{0Tag}}$	Predicted	127.9 ± 7.2	28.3 ± 2	30.2 ± 2.4	23.1 ± 2	4.96 ± 0.73	1.12 ± 0.38	4.5 ± 1.2
	Observed	116	35	29	21	3	1	5

Table 7: Observed and expected yields of SF events in the signal regions for the chargino search. The quoted uncertainty on the background predictions includes statistical and systematic contributions.

SF events	$M_{\mathrm{T2}}(\ell\ell)$ [GeV]	0-20	20-40	40-60	60-80	80-100	100-120	≥ 120
$\mathrm{SR1}^{\mathrm{Jets}}_{\mathrm{0Tag}}$	Predicted	1310 ± 29	499 ± 12	623 ± 14	634 ± 15	271.7 ± 8.9	51.6 ± 3.5	48.6 ± 5.5
	Observed	1324	499	609	659	284	57	47
$\mathrm{SR1}^{\mathrm{0Jet}}_{\mathrm{0Tag}}$	Predicted	44.1 ± 7.5	28.5 ± 4.1	33.5 ± 4.4	33.5 ± 4.5	18.6 ± 2.6	7.7 ± 1.6	12.5 ± 2.5
	Observed	43	40	39	33	17	6	12
$\mathrm{SR2}^{\mathrm{Jets}}_{\mathrm{0Tag}}$	Predicted	474 ± 14	134.8 ± 5.1	155.1 ± 5.5	128.5 ± 5.5	37.1 ± 2.5	7.29 ± 0.91	23.9 ± 2.4
	Observed	493	123	166	118	33	7	25
$\mathrm{SR2}^{\mathrm{0Jet}}_{\mathrm{0Tag}}$	Predicted	10.9 ± 1.9	7.8 ± 1.8	7.3 ± 1.4	7.9 ± 1.3	1.9 ± 0.52	1.28 ± 0.58	7.1 ± 1.4
	Observed	8	12	11	10	3	2	7
$\mathrm{SR3}_{\mathrm{0Tag}}$	Predicted	112.8 ± 6.3	27.9 ± 2.2	24.2 ± 1.8	22.5 ± 1.8	5.2 ± 1	1.36 ± 0.36	10.6 ± 1.2
	Observed	110	35	26	26	2	1	14

The 95% CL upper limits on the chargino pair production cross sections with the chargino

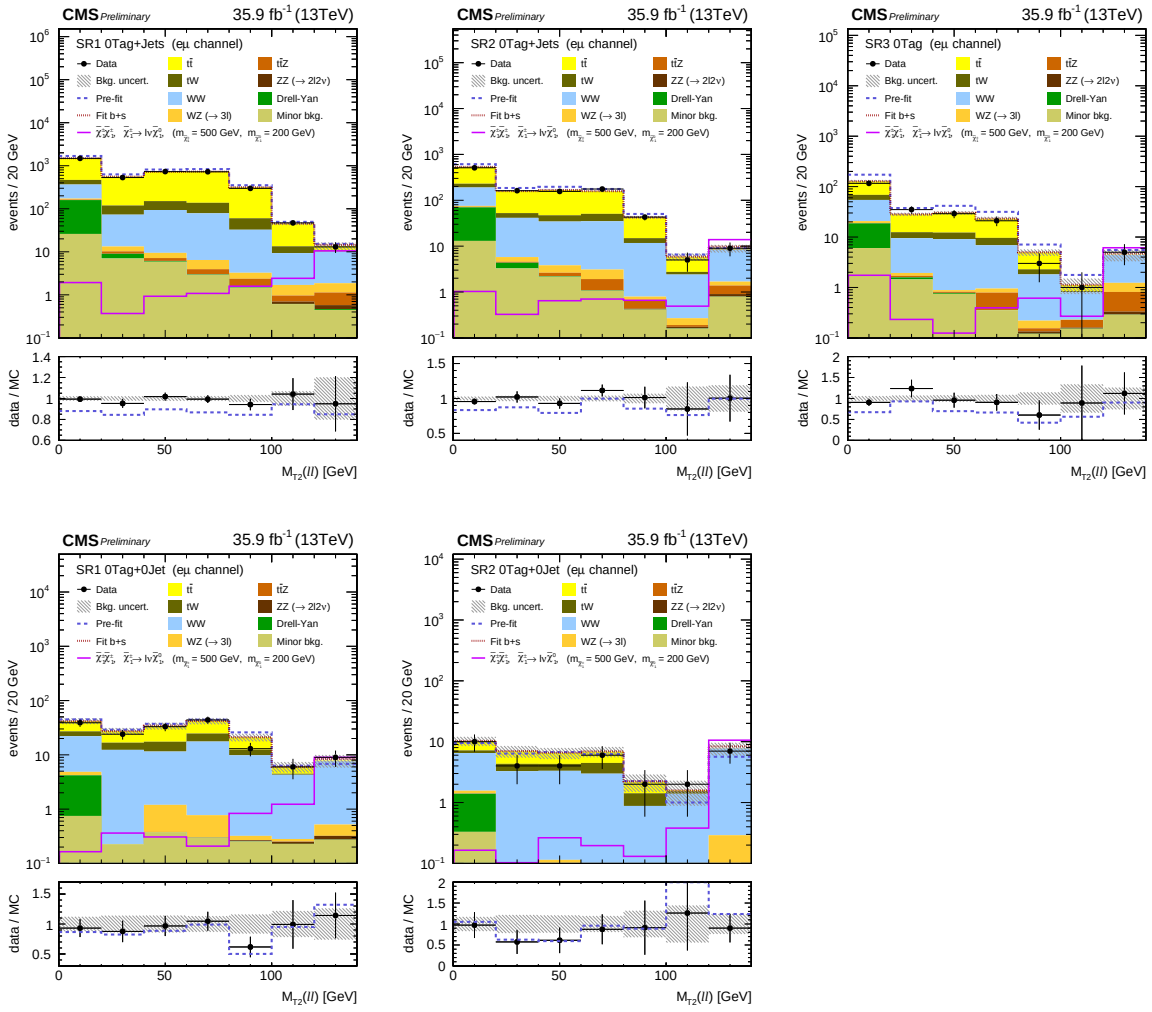

Figure 3: Distributions of $M_{\mathrm{T2}}(\ell\ell)$ after the fit to data in the chargino signal regions with $140 < p_{\mathrm{T}}^{\mathrm{miss}} < 200\,\mathrm{GeV}$ (left plots), $200 < p_{\mathrm{T}}^{\mathrm{miss}} < 300\,\mathrm{GeV}$ (middle) and $p_{\mathrm{T}}^{\mathrm{miss}} > 300\,\mathrm{GeV}$ (right), for DF events without b-tagged jets but at least one jet (upper plots) and no jets (lower plots). The upper plot for the signal region with $p_{\mathrm{T}}^{\mathrm{miss}} > 300\,\mathrm{GeV}$ shows all the events without b-tagged jets regardless of their jet multiplicity. Expected total SM contributions before the fit (dark blue dashed line) and after a background+signal fit (dark red dotted line) are also shown. The ratio data/MC is shown for the expected total SM contribution after the fit using the only background hypothesis (black dots) and before any fit (dark blue dashed line). The hatched band represents the total uncertainty after the fit.

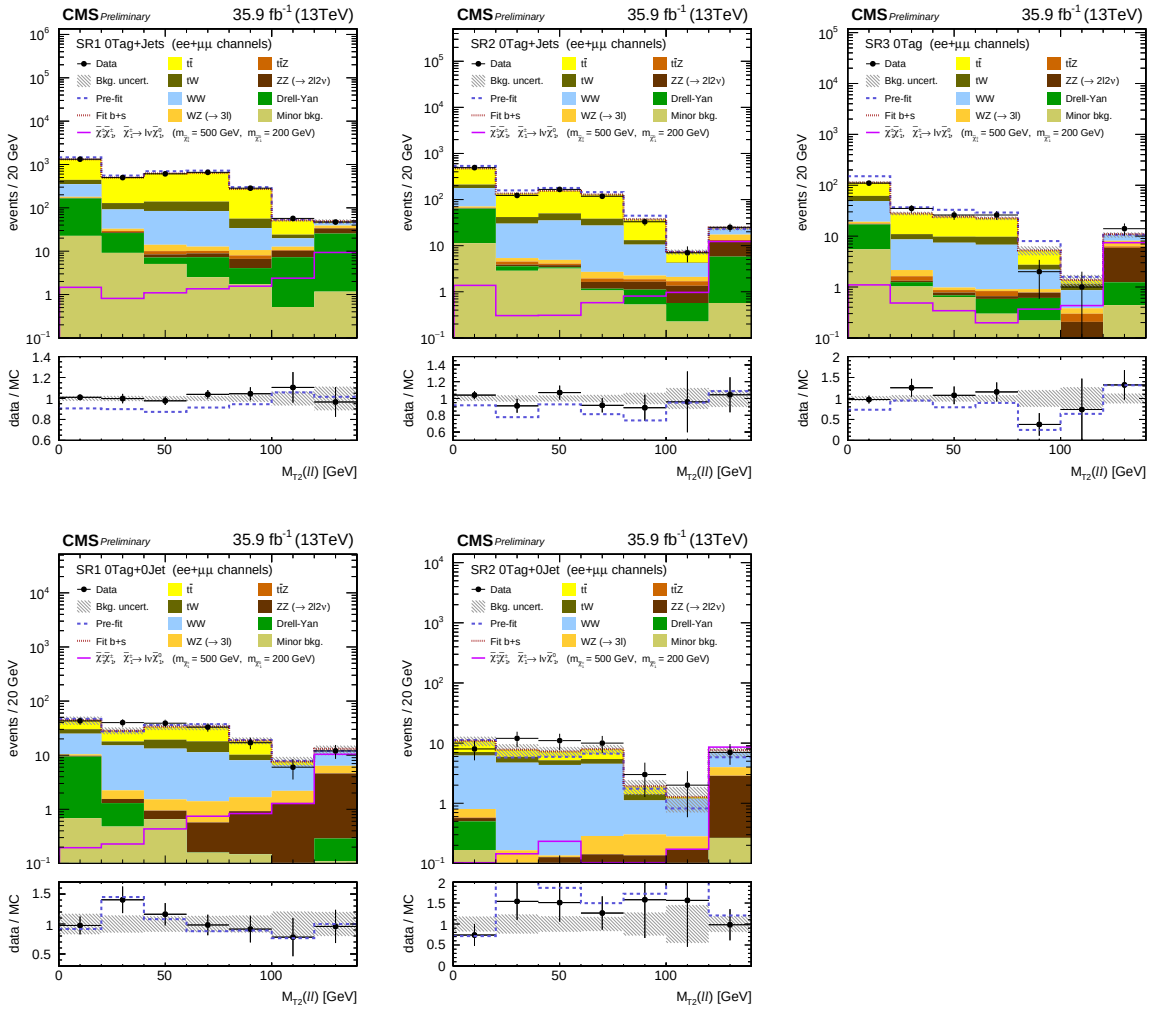

Figure 4: Distributions of $M_{\mathrm{T2}}(\ell\ell)$ after the fit to data in the chargino signal regions with $140 < p_{\mathrm{T}}^{\mathrm{miss}} < 200\,\mathrm{GeV}$ (left plots), $200 < p_{\mathrm{T}}^{\mathrm{miss}} < 300\,\mathrm{GeV}$ (middle) and $p_{\mathrm{T}}^{\mathrm{miss}} > 300\,\mathrm{GeV}$ (right), for SF events without b-tagged jets but at least one jet (upper plots) and no jets (lower plots). The upper plot for the signal region with $p_{\mathrm{T}}^{\mathrm{miss}} > 300\,\mathrm{GeV}$ shows all the events without b-tagged jets regardless of their jet multiplicity. Expected total SM contributions before the fit (dark blue dashed line) and after a background+signal fit (dark red dotted line) are also shown. The ratio data/MC is shown for the expected total SM contribution after the fit using the only background hypothesis (black dots) and before any fit (dark blue dashed line). The hatched band represents the total uncertainty after the fit.

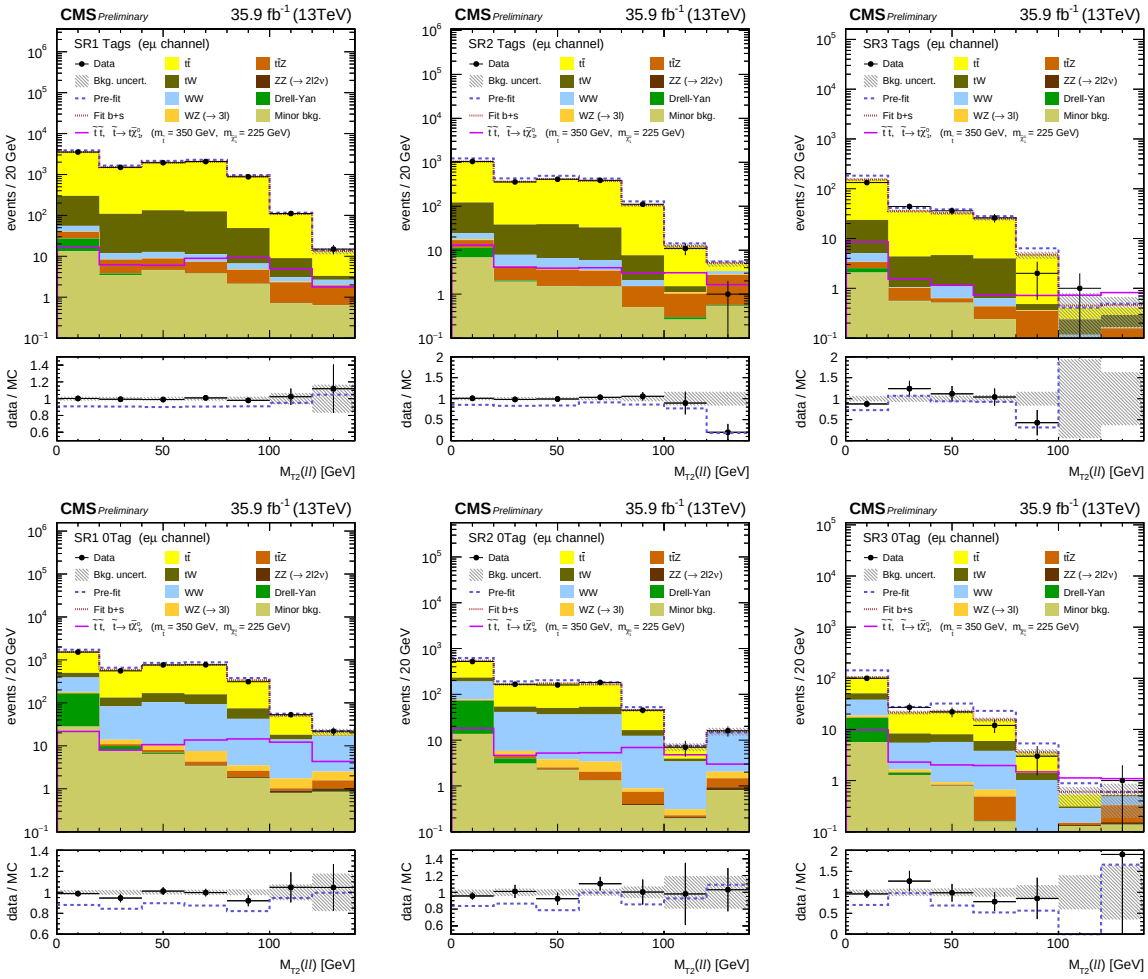

Figure 5: Distributions of $M_{\mathrm{T2}}(\ell\ell)$ after the fit to data in the top squark signal regions with $140 < p_{\mathrm{T}}^{\mathrm{miss}} < 200\,\mathrm{GeV}$ (left plots), $200 < p_{\mathrm{T}}^{\mathrm{miss}} < 300\,\mathrm{GeV}$ (middle), or $p_{\mathrm{T}}^{\mathrm{miss}} > 300\,\mathrm{GeV}$ (right), for DF events with b-tagged jets (upper plots) and without b-tagged jets (lower plots). Expected total SM contributions before the fit (dark blue dashed line) and after a background+signal fit (dark red dotted line) are also shown. The ratio data/MC is shown for the expected total SM contribution after the fit using the only background hypothesis (black dots) and before any fit (dark blue dashed line). The hatched band represents the total uncertainty after the fit.

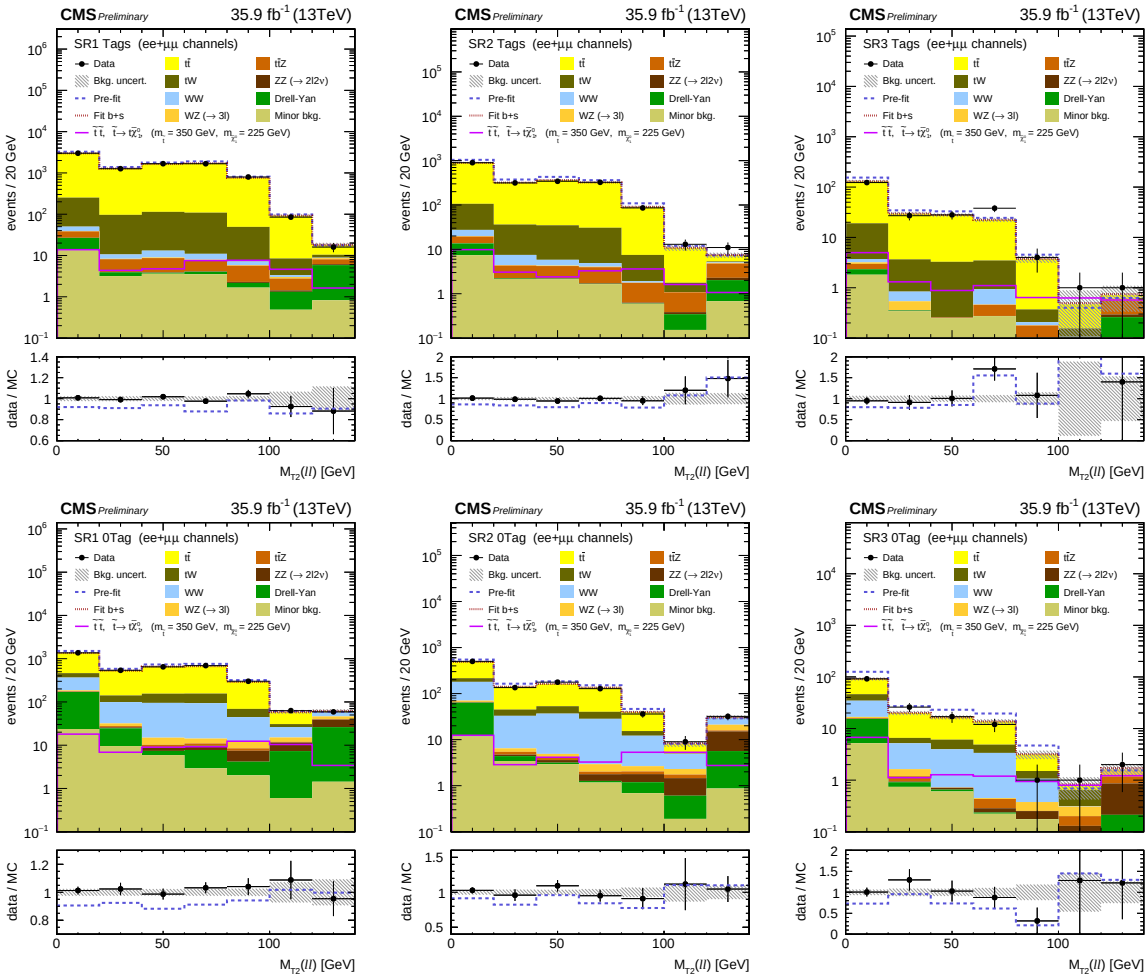

Figure 6: Distributions of $M_{\mathrm{T2}}(\ell\ell)$ after the fit to data in the top squark signal regions with $140 < p_{\mathrm{T}}^{\mathrm{miss}} < 200\,\mathrm{GeV}$ (left plots), $200 < p_{\mathrm{T}}^{\mathrm{miss}} < 300\,\mathrm{GeV}$ (middle), or $p_{\mathrm{T}}^{\mathrm{miss}} > 300\,\mathrm{GeV}$ (right), for SF events with b-tagged jets (upper plots) and without b-tagged jets (lower plots). Expected total SM contributions before the fit (dark blue dashed line) and after a background+signal fit (dark red dotted line) are also shown. The ratio data/MC is shown for the expected total SM contribution after the fit using the only background hypothesis (black dots) and before any fit (dark blue dashed line). The hatched band represents the total uncertainty after the fit.

Table 8: Observed and expected yields of DF events in the signal regions for the top squark search. The quoted uncertainty on the background predictions includes statistical and systematic contributions.

DF events	$M_{T2}(\ell\ell)$ [GeV]	0-20	20-40	40-60	60-80	80-100	100-120	≥ 120
$SR1_{Tags}$	Predicted	3525 ± 80	1505 ± 31	1958 ± 42	2049 ± 46	897 ± 22	108.4 ± 7.3	13.4 ± 2.2
	Observed	3534	1494	1938	2068	879	111	15
$SR1_{0Tag}$	Predicted	1542 ± 33	588 ± 13	756 ± 15	771 ± 19	338.3 ± 9.3	50.6 ± 3.8	21 ± 3.8
	Observed	1523	556	765	769	311	53	22
$SR2_{Tags}$	Predicted	1036 ± 37	363 ± 13	415 ± 14	377 ± 14	105.1 ± 6.5	12.3 ± 2	5.02 ± 0.82
	Observed	1045	357	412	389	111	11	1
$SR2_{0Tag}$	Predicted	545 ± 18	164.3 ± 7.3	173.2 ± 6.2	165.1 ± 6.8	44.8 ± 3.1	7.1 ± 1.4	15.5 ± 3
	Observed	521	166	160	182	45	7	16
$SR3^{ISR}_{Tags}$	Predicted	152.1 ± 9.9	35.5 ± 2.7	32.3 ± 2.3	25 ± 2.2	4.67 ± 0.77	0.41 ± 0.38	0.41 ± 0.26
	Observed	133	44	36	26	2	1	0
$SR3^{ISR}_{0Tag}$	Predicted	103.9 ± 6.8	21.3 ± 1.9	22.2 ± 2.1	15.4 ± 1.6	3.51 ± 0.6	0.53 ± 0.21	0.53 ± 0.34
	Observed	100	27	22	12	3	0	1

Table 9: Observed and expected yields of SF events in the signal regions for the top squark search. The quoted uncertainty on the background predictions includes statistical and systematic contributions.

SF events	$M_{T2}(\ell\ell)$ [GeV]	0-20	20-40	40-60	60-80	80-100	100-120	≥ 120
$SR1_{Tags}$	Predicted	2979 ± 68	1277 ± 30	1644 ± 35	1712 ± 37	762 ± 19	91.9 ± 6.1	18.1 ± 2.1
	Observed	3003	1266	1674	1671	798	85	16
$SR1_{0Tag}$	Predicted	1350 ± 33	526 ± 13	656 ± 15	670 ± 17	289.2 ± 7.6	57.9 ± 4.2	61.8 ± 5.8
	Observed	1367	539	648	692	301	63	59
$SR2_{Tags}$	Predicted	888 ± 30	319 ± 12	363 ± 14	323 ± 13	90.5 ± 5.5	10.8 ± 1.5	7.43 ± 0.98
	Observed	900	315	343	325	86	13	11
$SR2_{0Tag}$	Predicted	487 ± 16	140.7 ± 5.5	161.9 ± 5.9	134.5 ± 6.2	39.6 ± 2.7	8.1 ± 1.1	30.6 ± 3
	Observed	501	135	177	128	36	9	32
$SR3^{ISR}_{Tags}$	Predicted	129.6 ± 8.9	29.6 ± 2.1	27.8 ± 2.1	22.2 ± 1.9	3.71 ± 0.57	0.47 ± 0.42	0.71 ± 0.38
	Observed	123	27	28	38	4	1	1
$SR3^{ISR}_{0Tag}$	Predicted	91.5 ± 6.1	20.1 ± 1.8	16.5 ± 1.4	13.7 ± 1.4	3.14 ± 0.58	0.78 ± 0.36	1.63 ± 0.42
	Observed	92	26	17	12	1	1	2

decaying into sleptons are shown in Fig. 7 (left). The $\widetilde{\chi}_1^{\pm} \to \tilde{\ell}\nu \to \ell\nu\widetilde{\chi}_1^0$ and $\widetilde{\chi}_1^{\pm} \to \ell\tilde{\nu} \to \ell\nu\widetilde{\chi}_1^0$ decay chains are given a branching fraction of 50% each, and the sleptons are assumed to be degenerate, with a mass equal to the average of the chargino and neutralino masses. By comparing the upper limits with $pp \to \widetilde{\chi}_1^+\widetilde{\chi}_1^-$ production cross sections, observed and expected exclusion regions in the $(m_{\widetilde{\chi}_1^{\pm}}, m_{\widetilde{\chi}_1^0})$ plane are also determined. Masses are excluded up to values of about 800 GeV for the chargino and 320 GeV for the neutralino. Limited sensitivity is found when the chargino is assumed to decay into a W boson and the lighest neutralino, due to the relatively small branching fraction for the leptonic decay of the W boson. For this scenario, we derive upper limits on the chargino pair production cross section assuming a lightest neutralino mass of 1 GeV. Observed and expected upper limits as a function of the chargino mass are compared to theoretical cross sections in Fig. 7 (right).

Figure 8 shows the observed and expected 95% CL upper limits on the top squark production cross section for the two SMS considered. While the search strategy has been optimized for a compressed scenario, the results are presented on the whole $(m_{\tilde{t}}, m_{\widetilde{\chi}_1^0})$ plane for completeness. Also shown are the expected and observed exclusion regions when assuming NLO+NLL top

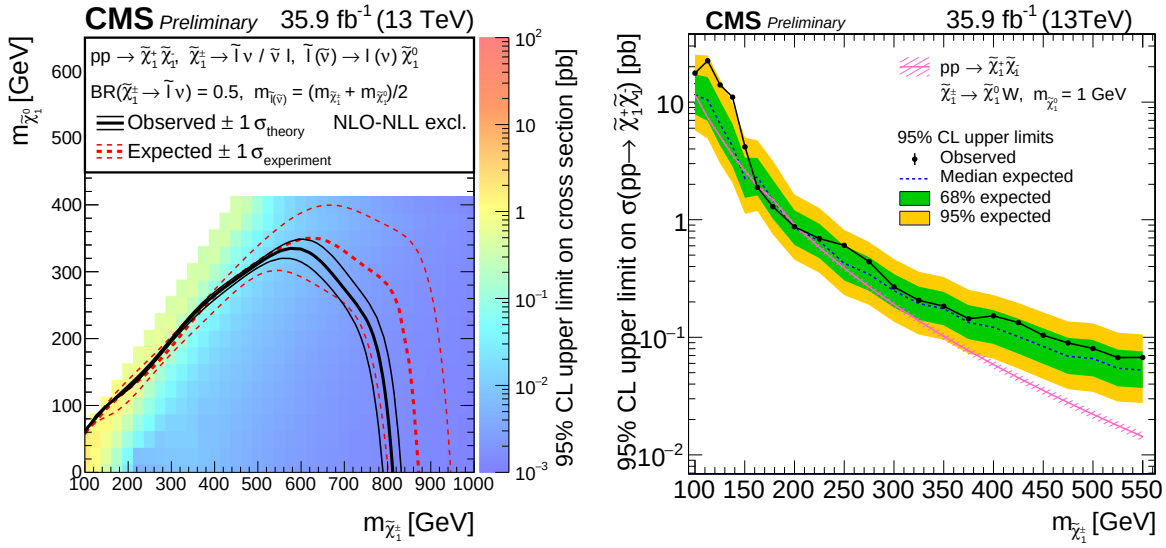

Figure 7: Left: upper limits at 95% CL on the chargino pair production cross section as a function of the chargino and neutralino masses, when the chargino undergoes a cascade decay $\widetilde{\chi}_1^{\pm} \to \tilde{\ell}\nu(\ell\widetilde{\nu}) \to \ell\nu\widetilde{\chi}_1^0$. The thick dashed red line shows the expected exclusion region in the plane $(m_{\widetilde{\chi}_1^{\pm}}, m_{\widetilde{\chi}_1^0})$. The thin dashed red lines show the variation of the exclusion regions due to the experimental uncertainties. The thick black line shows the observed exclusion region, while the thin black lines show the variation of the exclusion regions due to the theoretical uncertainties on the production cross section. Right: observed and expected upper limits at 95% CL as a function of the chargino mass for a neutralino mass of 1 GeV, assuming chargino decays into a neutralino and a W boson ($\widetilde{\chi}_1^{\pm} \to \mathrm{W}\widetilde{\chi}_1^0$).

squark pair production cross sections. In the compressed mass region where the analysis has been optimized, top squark masses are excluded up to about 420 (500) GeV for the $\tilde{t} \to t^* \tilde{\chi}_1^0$ ($\tilde{t} \to b\tilde{\chi}_1^{\pm} \to bW\tilde{\chi}_1^0$) decay mode. The uncovered region around a top squark mass of 200 GeV in Fig. 8 (right) corresponds to a signal phase space similar to that of $t\bar{t}$ events, with little contribution from the neutralino to the missing transverse energy. In this situation, the uncertainty in the modeling of $\vec{p}_T^{\,miss}$ in FastSim events becomes to turn off the signal sensitivity.

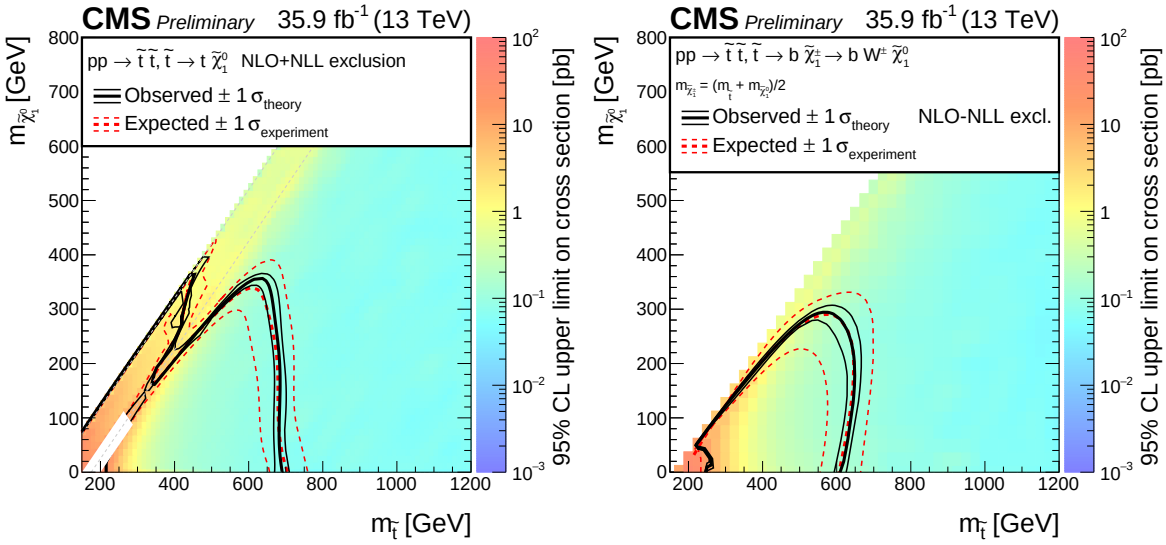

Figure 8: Upper limits at 95% CL on the top squark production cross section as a function of the stop and neutralino masses. The plot on the left shows the results when top squark decays into a top quark and a neutralino are assumed. The plot on the right gives the limits for top squarks decaying into a bottom quark and a chargino, with the latter successively decaying into a W boson and a neutralino. The mass of the chargino is assumed to be equal to the average of the top squark and neutralino masses. The thick dashed red line shows the expected exclusion region in the plane $(m_{\tilde{t}}, m_{\tilde{\chi}_1^0})$. The thin dashed red lines show the variation of the exclusion regions due to the experimental uncertainties. The thick black line shows the observed exclusion region, while the thin black lines show the variation of the exclusion regions due to the theoretical uncertainties on the production cross section.

9 Summary

A search has been presented for new physics in events with two oppositely charged isolated leptons and missing transverse momentum in 35.9 fb^{-1} of proton-proton collision data collected by the CMS detector during the 2016 run of the LHC operation at a center-of-mass energy of 13 TeV. No evidence for a deviation with respect to SM predictions was observed in data, and the results have been used to set upper limits on the cross section of supersymmetric particle production for several simplified supersymmetric model spectra.

The chargino pair production has been investigated in two possible decay modes. If the chargino is assumed to undergo a cascade decay through sleptons, an exclusion region in the $(m_{\tilde{\chi}_1^{\pm}}, m_{\tilde{\chi}_1^0})$ plane can be derived, extending till chargino masses of 800 GeV and neutralino masses of 320 GeV. These are the most stringent limits on this model to date. For chargino decays into a neutralino and a W boson, limits on production cross section have been derived assuming a neutralino mass of 1 GeV, and chargino masses in the range 170-200 GeV have been excluded.

Top squark pair production was also tested, with a focus on compressed decay modes. A model with the top squark decaying into a top quark and a neutralino was considered. In the region where $m_W < m_{\tilde{t}} - m_{\tilde{\chi}_1^0} \lesssim m_t$, top squark masses are excluded up to about 420 GeV. An alternative model has also been considered, where the top squark decays into a chargino and a bottom quark, with the chargino subsequently decaying into a W boson and the lightest neutralino. The results extend the previous exclusion region in the dilepton channel [27] in the compressed region where $175 \lesssim m_{\tilde{t}} - m_{\tilde{\chi}_1^0} \lesssim 225$ GeV up to a top squark mass of about 500 GeV.

References

[1] G. Bertone, D. Hooper, and J. Silk, "Particle dark matter: evidence, candidates and constraints", *Phys. Rept.* **405** (2005) 279, doi:10.1016/j.physrep.2004.08.031, arXiv:0404175.

[2] J. L. Feng, "Dark matter candidates from particle physics and methods of detection", *Ann. Rev. Astron. Astrophys.* **48** (2010) 495, doi:10.1146/annurev-astro-082708-101659, arXiv:1003.0904.

[3] T. A. Porter, R. P. Johnson, and P. W. Graham, "Dark matter searches with astroparticle data", *Ann. Rev. Astron. Astrophys.* **49** (2011) 155, doi:10.1146/annurev-astro-081710-102528, arXiv:1104.2836.

[4] P. Ramond, "Dual theory for free fermions", *Phys. Rev. D* **3** (1971) 2415, doi:10.1103/PhysRevD.3.2415.

[5] Y. A. Golfand and E. P. Likhtman, "Extension of the algebra of Poincaré group generators and violation of P invariance", *JETP Lett.* **13** (1971) 323.

[6] A. Neveu and J. H. Schwarz, "Factorizable dual model of pions", *Nucl. Phys. B* **31** (1971) 86, doi:10.1016/0550-3213(71)90448-2.

[7] D. V. Volkov and V. P. Akulov, "Possible universal neutrino interaction", *JETP Lett.* **16** (1972) 438.

[8] J. Wess and B. Zumino, "A Lagrangian model invariant under supergauge transformations", *Phys. Lett. B* **49** (1974) 52, doi:10.1016/0370-2693(74)90578-4.

[9] J. Wess and B. Zumino, "Supergauge transformations in four dimensions", *Nucl. Phys. B* **70** (1974) 39, doi:10.1016/0550-3213(74)90355-1.

[10] P. Fayet, "Supergauge invariant extension of the Higgs mechanism and a model for the electron and its neutrino", *Nucl. Phys. B* **90** (1975) 104, doi:10.1016/0550-3213(75)90636-7.

[11] Nilles, Hans Peter, "Supersymmetry, supergravity and particle physics", *Phys. Rep.* **110** (1984) 1, doi:10.1016/0370-1573(84)90008-5.

[12] G. t Hooft, "Naturalness, chiral symmetry, and spontaneous chiral symmetry breaking", *NATO Sci. Ser. B* **59** (1980) 135, doi:0.1007/978-1-4684-7571-5_9.

[13] E. Witten, "Dynamical breaking of supersymmetry", *Nucl. Phys. B* **188** (1981) 513, doi:10.1016/0550-3213(81)90006-7.

[14] S. Dimopoulos and H. Georgi, "Softly broken supersymmetry and SU(5)", *Nucl. Phys. B* **193** (1981) 150, doi:10.1016/0550-3213(81)90522-8.

[15] R. K. Kaul and P. Majumdar, "Cancellation of quadratically divergent mass corrections in globally supersymmetric spontaneously broken gauge theories", *Nucl. Phys. B* **199** (1982) 36, doi:10.1016/0550-3213(82)90565-X.

[16] G. R. Farrar and P. Fayet, "Phenomenology of the Production, Decay, and Detection of New Hadronic States Associated with Supersymmetry", *Phys. Lett. B* **76** (1978) 575, doi:10.1016/0370-2693(78)90858-4.

[17] CMS Collaboration, "The CMS experiment at the CERN LHC", *JINST* **3** (2008) S08004, doi:10.1088/1748-0221/3/08/S08004.

[18] J. Alwall, P. Schuster, and N. Toro, "Simplified models for a first characterization of new physics at the LHC", *Phys. Rev. D* **79** (2009) 075020, doi:10.1103/PhysRevD.79.075020, arXiv:0810.3921.

[19] J. Alwall, M.-P. Le, M. Lisanti, and J. G. Wacker, "Model-independent jets plus missing energy searches", *Phys. Rev. D* **79** (2009) 015005, doi:10.1103/PhysRevD.79.015005, arXiv:0809.3264.

[20] D. Alves et al., "Simplified models for LHC new physics searches", *J. Phys. G* **39** (2012) 105005, doi:10.1088/0954-3899/39/10/105005, arXiv:1105.2838.

[21] CMS Collaboration, "Searches for electroweak production of charginos, neutralinos, and sleptons decaying to leptons and W, Z, and Higgs bosons in pp collisions at 8 TeV", *Eur. Phys. J. C* **74** (2014) 3036, doi:10.1140/epjc/s10052-014-3036-7.

[22] ATLAS Collaboration, "Search for direct production of charginos, neutralinos and sleptons in final states with two leptons and missing transverse momentum in pp collisions at $\sqrt{s}$ = 8 TeV with the ATLAS detector", *JHEP* **1405** (2014) 071, doi:10.1007/JHEP05(2014)071.

[23] ATLAS Collaboration, "Search for the direct production of charginos, neutralinos and staus in final states with at least two hadronically decaying taus and missing transverse momentum in pp collisions at $\sqrt{s}$ = 8 TeV with the ATLAS detector", *JHEP* **1410** (2014) 096, doi:10.1007/JHEP10(2014)096.

[24] ATLAS Collaboration, "Search for the electroweak production of supersymmetric particles in $\sqrt{s}$ = 8 TeV pp collisions with the ATLAS detector", *Phys. Rev. D* **93** (2016) 052002, doi:10.1103/PhysRevD.93.052002.

[25] ATLAS Collaboration, "Search for the direct production of charginos and neutralinos in $\sqrt{s} = 13$ TeV pp collisions with the atlas detector", (2017). arXiv:1708.07875. Submitted to *Eur. Phys. J. C*.

[26] ATLAS Collaboration, "Search for electroweak production of supersymmetric states in scenarios with compressed mass spectra at $\sqrt{s} = 13$ TeV with the atlas detector", (2017). arXiv:1712.08119. Submitted to *Phys. Rev. D*.

[27] CMS Collaboration, "Search for top squarks and dark matter particles in opposite-charge dilepton final states at $\sqrt{s} = 13$ TeV", *Phys. Rev. D* **97** (2018) 032009, doi:10.1103/PhysRevD.97.032009, arXiv:1711.00752.

[28] CMS Collaboration, "Search for top squark pair production in pp collisions at $\sqrt{s} = 13$ TeV using single lepton events", *JHEP* **10** (2017) 019, doi:10.1007/JHEP10(2017)019, arXiv:1706.04402.

[29] CMS Collaboration, "Search for direct production of supersymmetric partners of the top quark in the all-jets final state in proton-proton collisions at $\sqrt{s} = 13$ TeV", *JHEP* **10** (2017) 005, doi:10.1007/JHEP10(2017)005, arXiv:1707.03316.

[30] ATLAS Collaboration, "Search for a scalar partner of the top quark in the jets plus missing transverse momentum final state at $\sqrt{s} = 13$ TeV TeV with the ATLAS detector", *JHEP* **12** (2017) 085, doi:10.1007/JHEP12(2017)085, arXiv:1709.04183.

[31] ATLAS Collaboration, "Search for top-squark pair production in final states with one lepton, jets, and missing transverse momentum using 36 fb^{-1} of $\sqrt{s} = 13$ TeV pp collision data with the ATLAS detector", (2017). arXiv:1711.11520. Submitted to *JHEP*.

[32] ATLAS Collaboration, "Search for direct top squark pair production in final states with two leptons in $\sqrt{s} = 13$ TeV pp collisions with the ATLAS detector", *Eur. Phys. J. C* **77** (2017) 898, doi:10.1140/epjc/s10052-017-5445-x, arXiv:1708.03247.

[33] CMS Collaboration, "The CMS trigger system", *JINST* **12** (2017) P01020, doi:10.1088/1748-0221/12/01/P01020, arXiv:1609.02366.

[34] P. Nason, "A new method for combining NLO QCD with shower Monte Carlo algorithms", *JHEP* **11** (2004) 040, doi:10.1088/1126-6708/2004/11/040, arXiv:0409146.

[35] S. Frixione, P. Nason, and C. Oleari, "Matching NLO QCD computations with parton shower simulations: the POWHEG method", *JHEP* **11** (2007) 070, doi:10.1088/1126-6708/2007/11/070, arXiv:0709.2092.

[36] S. Alioli, P. Nason, C. Oleari, and E. Re, "A general framework for implementing NLO calculations in shower Monte Carlo programs: the POWHEG BOX", *JHEP* **06** (2010) 043, doi:10.1007/JHEP06(2010)043, arXiv:1002.2581.

[37] M. Czakon and A. Mitov, "Top++: A Program for the Calculation of the Top-Pair Cross-Section at Hadron Colliders", *Comput.Phys.Commun.* **185** (2014) 2930, doi:10.1016/j.cpc.2014.06.021, arXiv:1112.5675.

[38] E. Re, "Single-top Wt-channel production matched with parton showers using the POWHEG method", *Eur. Phys. J. C* **71** (2011) 1547, doi:10.1140/epjc/s10052-011-1547-z, arXiv:1009.2450.

[39] T. Melia, P. Nason, R. Rontsch, and G. Zanderighi, "WW, WZ and ZZ production in the POWHEG BOX", *JHEP* **11** (2011) 078, doi:10.1007/JHEP11(2011)078, arXiv:1107.5051.

[40] P. Nason and G. Zanderighi, "WW, WZ and ZZ production in the POWHEG-BOX-V2", *Eur. Phys. J. C* **74** (2014) 2702, doi:10.1140/epjc/s10052-013-2702-5, arXiv:1311.1365.

[41] J. M. Campbell and R. K. Ellis, "MCFM for the Tevatron and the LHC", *Nucl. Phys. Proc. Suppl.* **205** (2010) 10, doi:10.1016/j.nuclphysbps.2010.08.011, arXiv:1007.3492.

[42] J. Alwall et al., "The automated computation of tree-level and next-to-leading order differential cross sections, and their matching to parton shower simulations", *JHEP* **07** (2014) 079, doi:10.1007/JHEP07(2014)079, arXiv:1405.0301.

[43] R. Gavin, Y. Li, F. Petriello, and S. Quackenbush, "FEWZ 2.0: A code for hadronic Z production at next-to-next-to-leading order", *Comput. Phys. Commun.* **182** (2011) 2388, doi:10.1016/j.cpc.2011.06.008, arXiv:1011.3540.

[44] M. V. Garzelli, A. Kardos, C. G. Papadopoulos, and Z. Trocsanyi, "$\text{t}\bar{\text{t}}\text{W}^{\pm}$ and $\text{t}\bar{\text{t}}\text{Z}$ hadroproduction at NLO accuracy in QCD with parton shower and hadronization effects", *JHEP* **11** (2012) 056, doi:10.1007/JHEP11(2012)056, arXiv:1208.2665.

[45] LHC Higgs Cross Section Working Group Collaboration, "Handbook of LHC Higgs Cross Sections: 3. Higgs Properties", (2013). arXiv:1307.1347.

[46] W. Beenakker et al., "Production of Charginos, Neutralinos, and Sleptons at Hadron Colliders", *Phys. Rev. Lett.* **83** (1999) 3780, doi:10.1103/PhysRevLett.83.3780, arXiv:hep-ph/9906298. [Erratum: *Phys. Rev. Lett.* **100** (2008) 029901, doi:10.1103/PhysRevLett.100.029901].

[47] B. Fuks, M. Klasen, D. R. Lamprea, and M. Rothering, "Gaugino production in proton-proton collisions at a center-of-mass energy of 8 TeV", *JHEP* **10** (2012) 081, doi:10.1007/JHEP10(2012)081, arXiv:1207.2159.

[48] B. Fuks, M. Klasen, D. R. Lamprea, and M. Rothering, "Precision predictions for electroweak superpartner production at hadron colliders with RESUMMINO", *Eur. Phys. J. C* **73** (2013) 2480, doi:10.1140/epjc/s10052-013-2480-0, arXiv:1304.0790.

[49] W. Beenakker, R. Hopker, M. Spira, and P. M. Zerwas, "Squark and gluino production at hadron colliders", *Nucl. Phys. B* **492** (1997) 51, doi:10.1016/S0550-3213(97)80027-2, arXiv:hep-ph/9610490.

[50] A. Kulesza and L. Motyka, "Threshold resummation for squark-antisquark and gluino-pair production at the LHC", *Phys. Rev. Lett.* **102** (2009) 111802, doi:10.1103/PhysRevLett.102.111802, arXiv:0807.2405.

[51] A. Kulesza and L. Motyka, "Soft gluon resummation for the production of gluino-gluino and squark-antisquark pairs at the LHC", *Phys. Rev. D* **80** (2009) 095004, doi:10.1103/PhysRevD.80.095004, arXiv:0905.4749.

[52] W. Beenakker et al., "Soft-gluon resummation for squark and gluino hadroproduction", *JHEP* **12** (2009) 041, doi:10.1088/1126-6708/2009/12/041, arXiv:0909.4418.

[53] W. Beenakker et al., "Squark and Gluino Hadroproduction", *Int. J. Mod. Phys. A* **26** (2011) 2637, doi:10.1142/S0217751X11053560, arXiv:1105.1110.

[54] C. Borschensky et al., "Squark and gluino production cross sections in pp collisions at $\sqrt{s}$ = 13, 14, 33 and 100 TeV", *Eur. Phys. J. C* **74** (2014) 3174, doi:10.1140/epjc/s10052-014-3174-y, arXiv:1407.5066.

[55] N. Collaboration, "Parton distributions for the LHC Run II", *JHEP* **04** (2015) 040, doi:10.1007/JHEP04(2015)040, arXiv:1410.8849.

[56] T. Sjstrand et al., "An Introduction to PYTHIA 8.2", *Comput. Phys. Commun.* **191** (2015) 159–177, doi:10.1016/j.cpc.2015.01.024, arXiv:1410.3012.

[57] C. Collaboration, "Event generator tunes obtained from underlying event and multiparton scattering measurements", *Eur. Phys. J. C* **76** (2016) 155, doi:10.1140/epjc/s10052-016-3988-x, arXiv:1512.00815.

[58] A. Kalogeropoulos and J. Alwall, "The SysCalc code: A tool to derive theoretical systematic uncertainties", (2018). arXiv:1801.08401.

[59] GEANT4 Collaboration, "GEANT4: A simulation toolkit", *Nucl. Instrum. Meth.* **A506** (2003) 250, doi:10.1016/S0168-9002(03)01368-8.

[60] CMS Collaboration, "The fast simulation of the CMS detector at LHC", *J.Phys.Conf.Ser.* **331** (2011) 032049, doi:10.1088/1742-6596/331/3/032049.

[61] CMS Collaboration, "Search for top-squark pair production in the single-lepton final state in pp collisions at sqrt(s) = 8 TeV", *Eur. Phys. J. C* **73** (2013) 2677, doi:10.1140/epjc/s10052-013-2677-2, arXiv:1308.1586.

[62] CMS Collaboration, "Particle-flow reconstruction and global event description with the CMS detector", *JINST* **12** (2017) P10003, doi:10.1088/1748-0221/12/10/P10003, arXiv:1706.04965.

[63] M. Cacciari, G. P. Salam, and G. Soyez, "The anti-k_t jet clustering algorithm", *JHEP* **04** (2008) 063, doi:10.1088/1126-6708/2008/04/063, arXiv:0802.1189.

[64] M. Cacciari, G. P. Salam, and G. Soyez, "FastJet user manual", *Eur. Phys. J. C* **72** (2012) 1896, doi:10.1140/epjc/s10052-012-1896-2, arXiv:1111.6097.

[65] CMS Collaboration, "Performance of electron reconstruction and selection with the CMS detector in proton-proton collisions at $\sqrt{s} = 8$ TeV", *JINST* **10** (2015) P06005, doi:10.1088/1748-0221/10/06/P06005, arXiv:1502.02701.

[66] CMS Collaboration, "Performance of CMS muon reconstruction in pp collision events at $\sqrt{s} = 7$ TeV", *JINST* **7** (2012) P10002, doi:10.1088/1748-0221/7/10/P10002, arXiv:1206.4071.

[67] CMS Collaboration, "Jet energy scale and resolution in the CMS experiment in pp collisions at 8 TeV", *JINST* **12** (2017) P02014, doi:10.1088/1748-0221/12/02/P02014, arXiv:1607.03663.

[68] CMS Collaboration, "Identification of heavy-flavour jets with the CMS detector in pp collisions at 13 TeV", (2017). arXiv:1712.07158. Submitted to *JINST*.

[69] C. G. Lester and D. J. Summers, "Measuring masses of semiinvisibly decaying particles pair produced at hadron colliders", *Phys. Lett.* **B463** (1999) 99–103, doi:10.1016/S0370-2693(99)00945-4, arXiv:hep-ph/9906349.

[70] CMS Collaboration, "CMS Luminosity Measurements at 13 TeV - Winter 2017 update", CMS Physics Analysis Summary CMS-PAS-LUMI-17-001, CERN, 2017.

[71] CMS Collaboration, "Measurement of differential cross sections for top quark pair production using the lepton+jets final state in proton-proton collisions at 13 TeV", *Phys. Rev. D* **95** (2017) 092001, doi:10.1103/PhysRevD.95.092001, arXiv:1610.04191.

[72] CMS Collaboration, "Measurement of the differential cross section for top quark pair production in pp collisions at $\sqrt{s} = 8$ TeV", *Eur. Phys. J. C* **75** (2015) 542, doi:10.1140/epjc/s10052-015-3709-x, arXiv:1505.04480.

[73] CMS Collaboration, "Measurement of the $\mathrm{t\bar{t}}$ production cross section in the all-jets final state in pp collisions at $\sqrt{s} = 8$ TeV", *Eur. Phys. J. C* **76** (2016) 128, doi:10.1140/epjc/s10052-016-3956-5, arXiv:1509.06076.

[74] A. Read, "Presentation of search results: the CLs technique", *J. Phys. G* **28** (2002) 2693, doi:10.1088/0954-3899/28/20/313.

[75] T. Junk, "Confidence level computation for combining searches with small statistics", *Nucl. Instrum. Meth. A* **434** (1999) 435, doi:10.1016/S0168-9002(99)00498-2, arXiv:9902006.

[76] G. Cowan, K. Cranmer, E. Gross, and O. Vitells, "Asymptotic formulae for likelihood-based tests of new physics", *Eur. Phys. J. C* **71** (2011) 1554, doi:10.1140/epjc/s10052-011-1554-0, arXiv:1007.1727. [Erratum: Eur. Phys. J.C73 (2013) 2501].